

## Strain Measurement in a Microstructure Using Digital Image Correlation for a Laser-Scanning Microscopic Image

N. Shishido, T. Ikeda, and N. Miyazaki

**Abstract:** We propose an image correction method that will accurately measure full-field displacement in a microstructure using the digital image correlation method (DICM); the proposed method is suitable for use with laser-scanned images. Laser scanning microscopes have higher spatial resolution and deeper depth of field than optical microscopes, but errors in laser scanning position (time-dependent distortion) affect the accuracy of the DICM. The proposed image correction method involves the removal of both time-dependant and time-independent distortions. Experimental results using images of prescribed rigid-body motions demonstrate that the proposed correction method is capable of identifying and removing both types of distortion. Specifically, the DICM employing the proposed image correction technique can eliminate both types of distortion in a laser-scanned image and measure full-field displacement within 0.04 pixel of the standard deviation. In addition, we used the proposed method to measure the thermal strain in both a copper specimen and a printed circuit board (PCB) during a thermal cycle test. For copper, the relative error between the measured strain and the reference strain is less than 0.0003 without the slant and bias of the strain field, which proves sufficient applicability of the developed system to measuring the distribution of strain caused by temperature change. The distribution of strain in the measured section of a PCB specimen was very complicated, but the average strain in the longitudinal direction showed good linearity. The variation in the average strain corresponds with that expected from beam theory for the macroscopic warpage of the PCB. This proves indirectly the accuracy of strain measurement using a laser microscope with the proposed method.

**Keyword:** Digital image correlation, strain measurement, correction, laser microscope.

## 1 Introduction

To reduce the size of electronic products, many kinds of electronic devices have been embedded in printed circuit boards (PCBs), which therefore contain many different materials (e.g., metals, resins, ceramics and composites). Composite material itself has a mesoscopic structure [Takashima, Nakagaki and Miyazaki (2007)], and other components of electronic devices induce complicated stress fields due to the mismatch of material properties. Such stress and strain around embedded devices affect the function of the devices [Hamada, Furusawa, Saito and Takeda (1991); Ali (1997)] and can cause the failure of electronic products [Ikeda, Arase, Ueno and Miyazaki (2000); Tay and Goh (2003)]. A system to measure stress and strain in microstructures is useful in order to evaluate the reliability of electronic devices. Laser interferometry techniques such as moiré interferometry and speckle interferometry are used to measure the distribution of strain in many structures [Guo, Lim, Chen and Woychik (1993); Laraba-Abbes, Ienny and Piques (2003)], and recently the digital image correlation method (DICM) has been used to measure displacement and strain in microregions because this technique is easy to use with a microscope [Li, Xu, Sutton and Mello (2006); Yan, Sutton, Deng and Cheng (2007)].

The DICM is an image-processing technique that can be used to determine the deformation of digital images. To achieve accurate measurement under a microscope, it is necessary to correct the image distortions before the DICM can be used. In the case of commonly used optical microscopes, an obtained image is spatially distorted by both the lens aberration and the slant of the sample arrangement. Many researchers have addressed the calibration of image distortion [Brown (1971); Lucchese (2005)]. Yoneyama, Kitagawa, Kitamura and Kikuta (2006) and Schreier, Garcia and Sutton (2004) achieved distortion correction for optical microscopic images applied to the DICM using a cross-grating pattern and a set of rigid-body motions, respectively.

In addition to the distortion based on the optics, there are other distortions in images obtained using a scanning microscope that can observe at magnifications higher than  $1000\times$  (e.g., laser scanning microscopes, scanning electron microscopes, and atomic force microscopes). Since the scanning procedure causes a complicated distribution of distortion that depends on time and space, a new model and a calibration procedure to eliminate these distortions are necessary. An image obtained using an atomic force microscope (AFM) is dominantly affected by thermal drift due to both the slow scan-rate and the higher magnification. Sun and Pang (2006) proposed a method to remove thermal drift distortion in an AFM image using two scan-directions orthogonal to each other. An image obtained using a scanning electron microscope (SEM) includes spatial distortion, thermal drift distortion, and

other disorder distortions that strongly depend on the apparatus. Sutton, Li, Garcia, Cornille, Orteu, McNeill, Schreier and Li (2006) removed the thermal drift distortion from an obtained image using a set of time-series images, and a disorder distortion, which Sutton, Li, Joy, Reynolds and Li (2007) called as a step change, was eliminated throughout multiple scanning. A laser-scanning microscope (LSM) can neglect thermal drift, due to its higher scan-rate than those of other scanning microscopes. However, there is a measurable disorder-distortion and a complex spatial-distortion in the image obtained using an LSM. An LSM has higher spatial resolution and deeper depth of field than those of other optical microscope, but it has a scanning position error (time-dependent distortion), and a suitable calibration technique to eliminate time-dependent distortion is necessary.

In this paper, we propose an image correction method that is suitable for use with LSM images, which is effective to measure accurate full-field displacement in a microstructure using the DICM. This correction procedure involves the removal of both time-dependant and time-independent distortions using the DICM. The results of our experiments, which used prescribed rigid-body motions, demonstrate that this correction method is capable of identifying and removing both types of distortion. In addition, we applied the present method to the measurement of thermal deformation in a copper specimen and in a printed circuit board (PCB) during a thermal cycle test and verified the reliability of the present method in considering the relationship between macroscopic and microscopic PCB deformations.

## 2 Digital image correlation

In this study, we measured displacement using the DICM proposed by Bruck, McNeill, Sutton and Peters (1989). The DICM determines the displacement at the center of a small area, which is called a subset, by comparing two digital images. These images are usually obtained before and after deformation. In the image obtained before deformation, a rectangular area is defined as a reference subset, and the point of interest is located at the center of it. In a subset of the image obtained after deformation, the correlation with the reference subset is evaluated using the distribution of light intensity. The subset that has the highest correlation with the reference subset can be determined as the deformed subset that corresponds with the reference subset before deformation. Evaluating the correlation between subsets, the object function is defined as

$$C = \frac{\sum_{i, j=-M}^M I_d(X+i, Y+j) \times I_u(x+i, y+j)}{\sqrt{\sum_{i, j=-M}^M I_d(X+i, Y+j)^2 \sum_{i, j=-M}^M I_u(x+i, y+j)^2}} \quad (1)$$

which is known as the cross-correlation function.  $I_u(x, y)$  is the light intensity at coordinate  $(x, y)$  for the reference image, and  $I_d(X, Y)$  is the light intensity at the coordinate  $(X, Y)$  for the deformed image.  $(x, y)$  and  $(X, Y)$  are related by the deformation,

$$X = x + u + \frac{\partial u}{\partial x}i + \frac{\partial u}{\partial y}j, \quad Y = y + v + \frac{\partial v}{\partial x}i + \frac{\partial v}{\partial y}j \quad (2)$$

where  $u$  and  $v$  are the displacement at the center of a subset in the  $x$  and  $y$  directions, respectively;  $\partial u/\partial x$ ,  $\partial u/\partial y$ ,  $\partial v/\partial x$ , and  $\partial v/\partial y$  are the constant gradient terms in the deformed subset;  $i$  and  $j$  represent the local coordinates in a subset, and  $M$  is the size of a reference subset. The Newton-Raphson method is performed to determine  $u$ ,  $v$ ,  $\partial u/\partial x$ ,  $\partial u/\partial y$ ,  $\partial v/\partial x$ , and  $\partial v/\partial y$  that maximize the object function  $C$ .

### 3 Image distortions in a laser-scanning microscope

The displacement measured using the DICM is affected by the underlying distortions of the images. To estimate the displacement due to the deformation of the object accurately, the distortions of the images must be evaluated and eliminated from the images. According to the pre-experimental results, we divided the distortion into two components to enable the best reproducibility of these distortions.  $\mathbf{D}_T$  was defined as the time-dependent distortion induced by the fluctuation of the scanning trajectory, and  $\mathbf{D}_S$  was defined as the time-independent distortion due to a constant position error. We separately estimated each component via a novel procedure so that the undistorted image could be obtained using the inverse function of these components. The ideal position  $\mathbf{r}_{id} = (x_{id}, y_{id})^T$  of the point can be written as follows:

$$\mathbf{r}_{im} = \mathbf{r}_{id} + \mathbf{D}_T(\mathbf{r}_{im}) + \mathbf{D}_S(\mathbf{r}_{im}) \quad (3)$$

where  $\mathbf{r}_{im} = (x_{im}, y_{im})^T$  shows the position on the image plane that has the distortions.

#### 3.1 Time-dependent distortion

Time-dependent distortion in an LSM image is induced by deviation of the scan trajectory due to the limit of its controllability. This deviation leads to a difference between the true position and the apparent position of the laser beam on the specimen surface for each moment of scanning. In the LSM system employed in this study, the OLYMPUS OLS3000, deviation occurs randomly for each separate scan-line toward the scanning direction (usually the horizontal direction, as shown in Fig. 1(a)), while deviation toward the vertical direction may be negligible. Thermal drift and mechanical vibrations are negligibly small for the distortion because

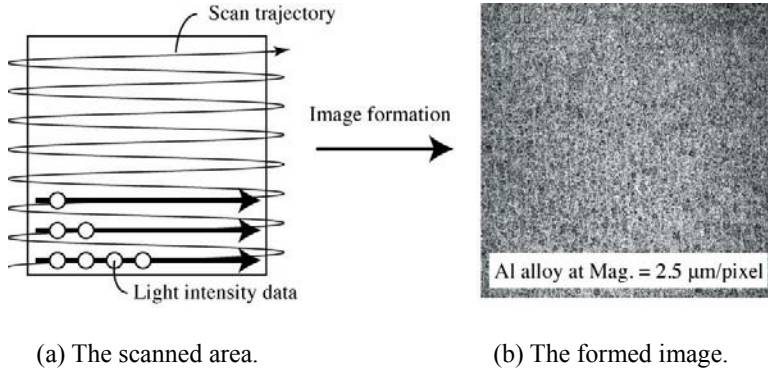


Figure 1: Schematic diagram of the image formation process in a laser-scanning microscope. Light intensity data are sampled in 12-bit lengths on a  $1024 \times 1024$  grid array.

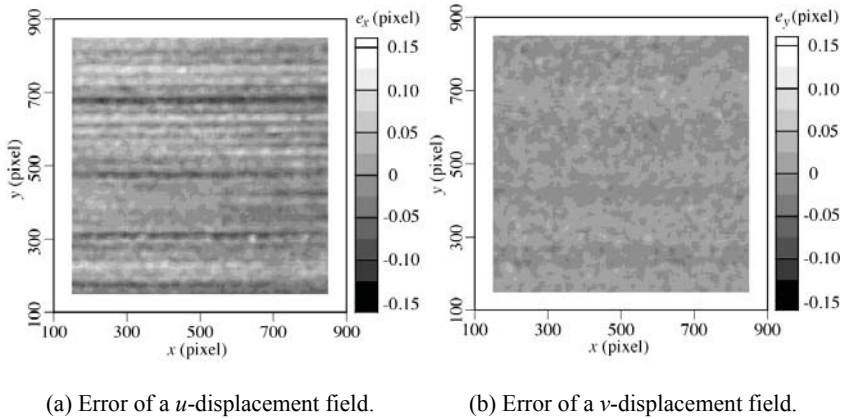


Figure 2: The error of relative displacement between stationary statements  $\mathbf{t}_{pre} = (0 \mu\text{m}, 0 \mu\text{m})^T$ . The subset size,  $M$ , is 10 pixels.

of the higher scan-rate (4000 Hz) and relatively lower magnification ( $\sim 1000\times$ ) of this microscope compared to those of other scanning microscopes. These assumptions agree closely with experimental observations, in which apparent displacement occurred between stationary images, as shown in Figs. 2(a) and 2(b). Thus, the components of the time-dependent distortion can be written as follows:

$$D_T(r_{im}) = [D_{Tx}(y_{im}), 0]^T \quad \text{at } y_{im} = 1, 2, \dots \quad (4)$$

The function  $\mathbf{D}_T$  depends on the direction of laser scanning. Thus, a pair of images

with different scanning directions, especially those orthogonal to each other, is used to determine  $\mathbf{D}_T$  for both the reference image and the deformed image. A vertically scanned image (perpendicular to the usual scan direction) has a different distortion, which is written as follows:

$$D_T(r_{im}) = [0, D_{Ty}(x_{im})]^T \quad \text{at } x_{im} = 1, 2, \dots \quad (5)$$

For a pair of images that show the same region, the difference in the distortions between images is equivalent to the relative displacement  $\Delta \mathbf{r}_{im} = (U, V)^T$ , which is written using Eqs. (3) ~ (5), as follows:

$$\Delta \mathbf{r}_{im} = [-D_{Tx}(y_{im}), D_{Ty}(x_{im})]^T \quad (6)$$

Estimating  $\Delta \mathbf{r}_{im}$  experimentally, we performed the DICM using a horizontally scanned image as the reference image and a vertically scanned image as the deformed image. Under the assumption that  $\Delta \mathbf{r}_{im}$  is equivalent to the displacement measured by the DICM, Sun and Pang (2006) determined the time-dependent distortion induced by the scanner drift of an AFM, which changes gradually in an AFM image. However, the displacement measured by the DICM based on Eqs. (1) and (2) is not sufficient to estimate  $\mathbf{D}_T$  for an LSM image whose  $\mathbf{D}_T$  occurs randomly on scanned lines, because the DICM based on Eqs. (1) and (2) obtains an averaged displacement within a subset region [Schreier and Sutton (2002)]. Thus, we determined  $\mathbf{D}_T$  more accurately using a modified function,  $C_M$ , which is defined as

$$C_M = \sum_{i, j=-M}^M \frac{I_d(X+i, Y+D_{Ty}+j)}{\sum_{i, j=-M}^M I_d(X+i, Y+D_{Ty}+j)^2} \times \frac{I_u(x+D_{Tx}+i, y+j)}{\sum_{i, j=-M}^M I_u(x+D_{Tx}+i, y+j)^2} \quad (7)$$

Both the six variables of the deformation of a subset and the  $4M+2$  values of  $D_{Tx}$  and  $D_{Ty}$  are obtained when  $C_M$  has the highest correlation value. The modified function  $C_M$  is employed in the DICM using a pair of images that are focused on the same region with orthogonal scan directions.

### 3.2 Time-independent distortion

The time-independent distortion in an LSM image is induced by both the classical deviation based on the optical system [Brown (1971); Lucchese (2005); Yoneyama, Kitagawa, Kitamura and Kikuta (2006)] and the disparity of a pixel position between the grid array of an image plane and the sampled points on an oscillatory scan trajectory. Parametric forms for distortion models, which originated in the classic models (e.g., radial distortion, decentering distortion, and so on), are not

preferred to correct the unknown distortion [Schreier, Garcia and Sutton (2004); Sutton, Li, Garcia, Cornille, Orteu, McNeill, Schreier and Li (2006)]. The effect of the distortion occurs with much complexity in space, as shown in the experimental results for the rigid body motions (Fig. 3(a)(b)).

The translation along the  $x$ -axis generated the vertical stripe in the shape of the relative displacement map  $e_x$ , in addition to the effect of the time-dependent distortion (Fig. 3(a)), and the translation along the  $y$ -axis generated the horizontal stripe in the shape of the displacement map  $e_y$  (Fig. 3(b)). Based on these results, it can be assumed that the time-independent distortion  $\mathbf{D}_S$  consists of two functions, as follows:

$$D_S(r_{im}) = D_S^0(r_{im}) + D_S^1(r_{im}) \quad (8)$$

where  $D_S^0$  is the distortion which is caused by the deviation of an optical system, and depends on the position, as follows:

$$D_S^0(r_{im}) = [D_{Sx}^0(x_{im}, y_{im}), D_{Sy}^0(x_{im}, y_{im})]^T \quad (9)$$

$D_S^1$  is the distortion which is caused by the disparity of pixel position. Similar to the time-dependent distortion shown in Eqs. (4)-(6), the  $x$ -component and  $y$ -component of  $D_S^1$  depend on  $x_{im}$  and  $y_{im}$ , respectively, as follows:

$$D_S^1(r_{im}) = [D_{Sx}^1(x_{im}), D_{Sy}^1(y_{im})]^T \quad (10)$$

$D_S^0$  is assumed to gradually change in space, and it can be obtained by conventional procedures [Schreier, Garcia, and Sutton (2004); Sutton, Li, Garcia, Cornille, Orteu, McNeill, Schreier and Li (2006)]. Each function is separately estimated throughout several rigid-body motions as follows. The relative displacement  $\Delta \mathbf{r}_{im}$  for an arbitrary translation  $\mathbf{t}_{pre}$  can be written as

$$\begin{aligned} \Delta r_{im} = & t_{pre} + D_T(r_{im} + \Delta r_{im}) - D_T(r_{im}) \\ & + D_S^0(r_{im} + \Delta r_{im}) - D_S^0(r_{im}) \\ & + D_S^1(r_{im} + \Delta r_{im}) - D_S^1(r_{im}) \end{aligned} \quad (11)$$

with

$$r_{id} \rightarrow r_{id} + t_{pre}, \quad t_{pre} = [u_{pre}, v_{pre}]^T \quad (12)$$

where  $u_{pre}$  and  $v_{pre}$  represent the prescribed displacements along the  $x$  and  $y$  axes due to a translation, respectively. The displacement  $\Delta \mathbf{r} = (u, v)$  measured using the large subset-size  $M$  for the DICM can neglect the effect of high-frequency distributing distortions such as  $\mathbf{D}_T$  and  $D_S^1$  [Schreier and Sutton (2002)], when applying a

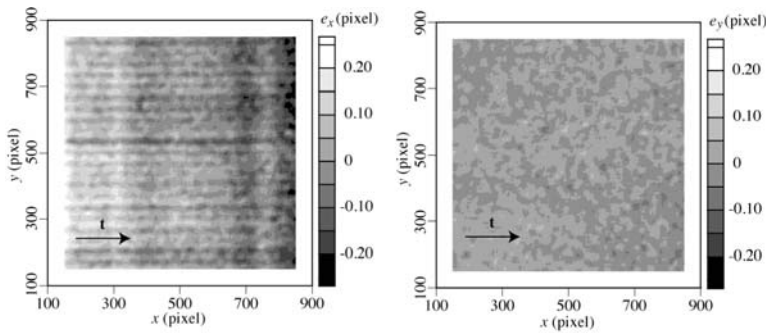
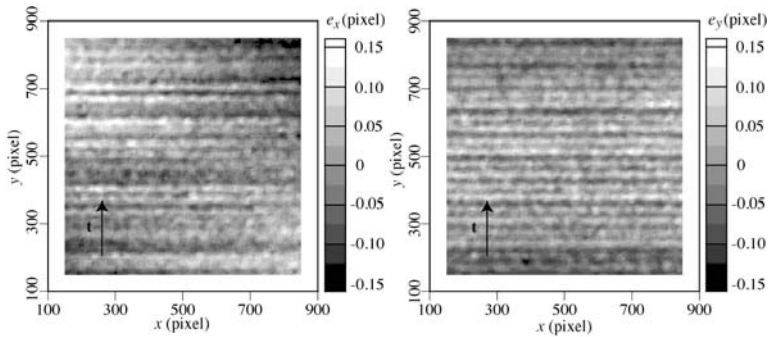
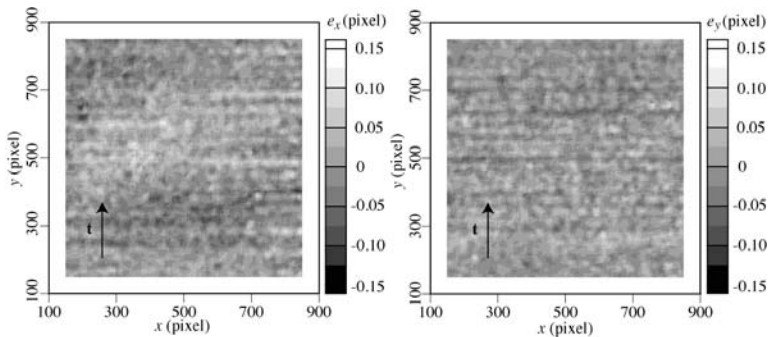
(a) Error of displacement fields for  $\mathbf{t}_{\text{pre}} = (50 \mu\text{m}, 0 \mu\text{m})^T$ . Left:  $e_x$ , right:  $e_y$ .(b) Error of displacement fields for  $\mathbf{t}_{\text{pre}} = (0 \mu\text{m}, 50 \mu\text{m})^T$ . Left:  $e_x$ , right:  $e_y$ .(c) Error of displacement fields with image correction for (b). Left:  $e_x$ , right:  $e_y$ .

Figure 3: Errors of relative displacement for translations, which are equivalent to “ $\Delta\mathbf{r} - \mathbf{t}_{\text{pre}}$ ”. The subset size  $M$  is 10 pixels, and the magnification is  $2.5 \mu\text{m}/\text{pixel}$ .  $e_x$ , error of  $x$ -displacement;  $e_y$ , error of  $y$ -displacement.

sufficiently large  $M$  for measuring displacements. Eq. (9) is rewritten using  $\Delta \mathbf{r}_{\text{LM}}$ , which is the measured displacement using the DICM with large  $M$ , as follows:

$$\Delta r_{\text{LM}} = t_{\text{pre}} + D_{\text{S}}^0(r_{\text{im}} + \Delta r) - D_{\text{S}}^0(r_{\text{im}}) \quad (13)$$

The displacement field  $\Delta \mathbf{r}(\mathbf{r}_{\text{im}})$  is obtained by the moving least squares method (MLSM), which interpolates values between discrete points and generates smooth distribution in data space (e.g. [Lancaster and Salkauskas (1981)][Nie, Atluri and Zuo (2006)]). Based on Eq. (13),  $D_{\text{S}}^0$  on the photographic field  $\mathbf{r}_{\text{im}}$  can be estimated recursively, as follows:

$$D_{\text{S}}^0(r_{\text{im}}^{n+1}) = D_{\text{S}}^0(r_{\text{im}}^n) + \Delta r(r_{\text{im}}^n) - t_{\text{pre}} \quad (14)$$

with

$$r_{\text{im}}^{n+1} = r_{\text{im}}^n + \Delta r(r_{\text{im}}^n), \quad r_{\text{im}}^n = [x_{\text{im}}^n, y_{\text{im}}^n]^T \quad n = 1, 2, \dots \quad (15)$$

The displacement field between before and after translation along the  $x$ -axis provides the series of  $D_{\text{S}}^0$  along the  $x$ -axis at interval  $\Delta \mathbf{r}$ , starting from  $r_{\text{im}}^1$ . Combining the  $x$ -axis and  $y$ -axis translations, we can obtain the values  $D_{\text{S}}^0$  on the grid-array points and estimate the distortion map of  $D_{\text{S}}^0$  on the photographic field using the MLSM.

Using the obtained distortion  $D_{\text{S}}^0$ , the determination of  $D_{\text{S}}^1$  is performed by the same procedures with the small subset  $M$  applied to the DICM. Employing the partly corrected image, from which the effect of  $D_{\text{S}}^0$  is eliminated,  $\Delta \mathbf{r}_{\text{SM}}$ , which is the measured displacement using the DICM with small  $M$ , is obtained from Eq. (11) as follows:

$$\Delta r_{\text{SM}} = t_{\text{pre}} + \begin{bmatrix} D_{\text{Tx}}^D(y_{\text{im}} + v) - D_{\text{Tx}}^R(y_{\text{im}}) \\ + D_{\text{Sx}}^1(x_{\text{im}} + u) - D_{\text{Sx}}^1(x_{\text{im}}) \\ D_{\text{Sy}}^1(y_{\text{im}} + v) - D_{\text{Sy}}^1(y_{\text{im}}) \end{bmatrix} \quad (16)$$

where  $D_{\text{Tx}}^R$  and  $D_{\text{Tx}}^D$  show the time-dependent distortions that occur in the reference image and the image after deformation, respectively. The recursive estimation of  $D_{\text{Sy}}^1$  is performed using the  $y$ -displacement map  $\Delta r_{\text{SM}y}(\mathbf{r}_{\text{im}})$  obtained by the DICM using the small subset, as follows:

$$D_{\text{Sy}}^1(y_{\text{im}}^{n+1}) = D_{\text{Sy}}^1(y_{\text{im}}^n) + \Delta r_{\text{SM}y}(x_{\text{im}}^n, y_{\text{im}}^n) - t_{\text{pre}y} \quad (17)$$

where  $t_{\text{pre}y}$  is the  $y$ -component of  $\mathbf{t}_{\text{pre}}$ . Since the series of  $D_{\text{Sx}}^1$  along the  $y$ -axis has the intervals about  $\Delta \mathbf{r}$ , the small translation  $\mathbf{t}_{\text{pre}}$  is preferred to generate the distribution of  $D_{\text{Sx}}^1$  accurately by using the MLSM. Considering the experimental results,

it can be assumed that the averaged value of  $D_{Tx}$  along the  $y$ -axis is almost zero. Under this assumption,  $D_{Sx}^1$  is estimated recursively using the following equation:

$$D_{Sx}^1(x_{im}^{n+1}) = D_{Sx}^1(x_{im}^n) + \Delta r_{SMx}(x_{im}^n) - p_{prex} \quad (18)$$

where  $\Delta r_{SMx}$  and  $p_{prex}$  are  $x$ -components of  $\Delta \mathbf{r}_{SM}$  and  $\mathbf{p}_{pre}$ , respectively. Eq. (18) is derived by averaging Eq. (16) along the  $y$ -axis, and  $\Delta r_{SMx}(x_{im}^n)$  is defined as the averaged value of the measured displacement  $\Delta r_{SMx}(x_{im}^n, y_{im}^n)$  along the  $y$ -axis.

### 3.3 Procedure of distortions correction

The procedure to estimate the time-independent distortion,  $\mathbf{D}_S$ , requires only three images, one reference image and two images moved along two orthogonal directions with a motorized stage. Two relative displacement fields are measured and employed for generating the map of  $\mathbf{D}_S$  using the MLSM. After that, the time-dependent distortions  $\mathbf{D}_T$  before and after deformation can be determined using a pair of images with the orthogonal scan-direction for each statement. The modified function  $C_M$  determines respective  $\mathbf{D}_T$  of images scanned in orthogonal directions throughout the DICM. The estimation of  $\mathbf{D}_S$  is required only once for the same magnification of an LSM due to its stationary nature. In contrast, the estimation of  $\mathbf{D}_T$  is required for each measurement. In other words, four images are required for the DICM in order to measure object deformation without the effects of the time-dependents.

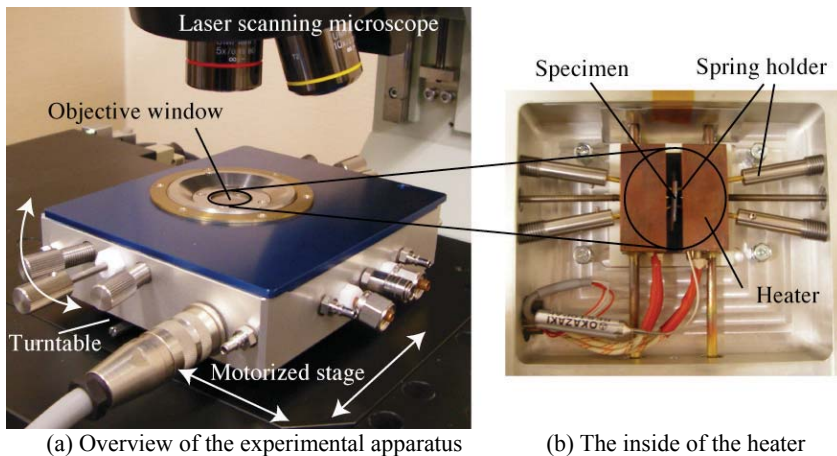


Figure 4: Photographs of an experimental apparatus.

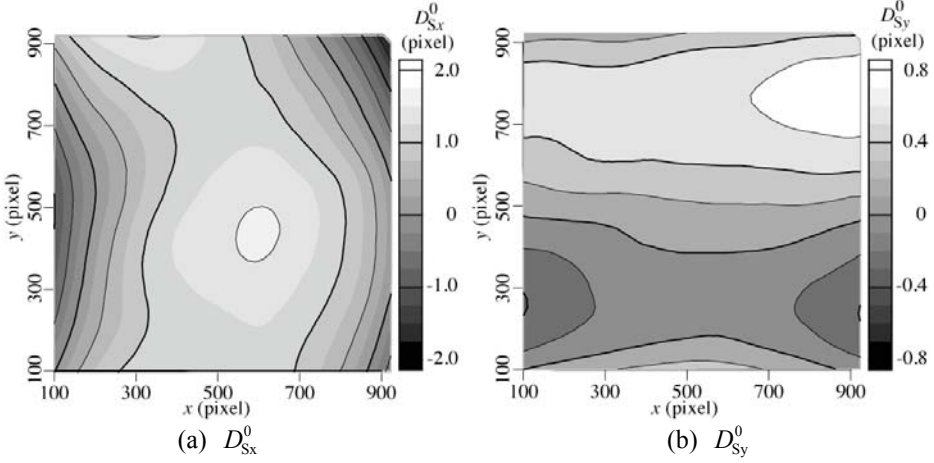


Figure 5: Distortion map of  $D_{\Sigma}^0$ . The subset size  $M$  is 75 pixels, and the magnification is  $2.5 \mu\text{m}/\text{pixel}$ .

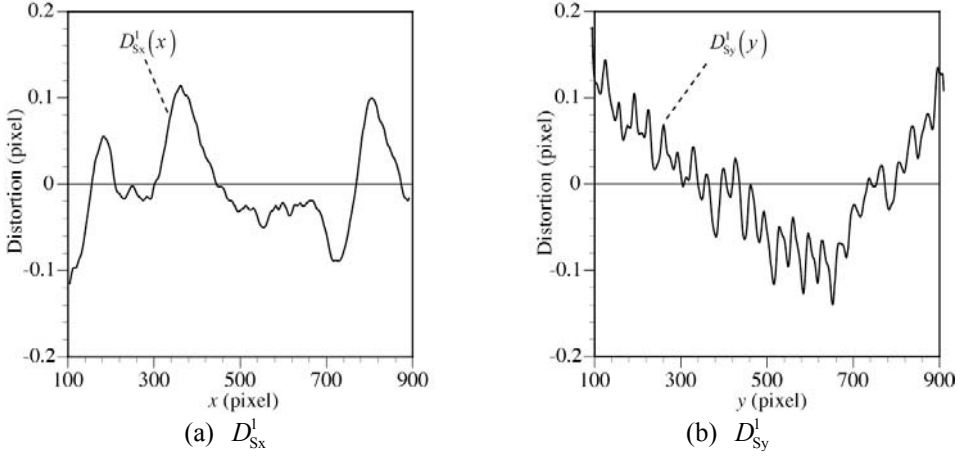


Figure 6: Distortion functions of  $D_{\Sigma}^1$ . The subset size  $M$  is 2 pixels and the magnification is  $2.5 \mu\text{m}/\text{pixel}$ .

## 4 Experiment

### 4.1 Measurement of rigid-body motions

To validate the proposed correction method, we corrected several images obtained using an LSM and examined the accuracy of the correction method. The apparatus is shown in Fig. 4. The specimen was patterned so that LSM images were appropri-

ate for the DICM, as shown in Fig. 1(b). The size of the array was  $1024 \times 1024$ , and the magnification of the image was  $2.5 \mu\text{m}/\text{pixel}$ . To make the time-independent distortion map,  $\mathbf{D}_S$ , we generated a series of translations in two orthogonal directions using a motorized stage, which belongs to the LSM system and has about  $1 \mu\text{m}$  reproducibility. Figures 5 and 6 show the obtained distortion maps for translations of  $16 \mu\text{m}$  along the  $x$ - and  $y$ -axes. Image correction using the distortion map  $\mathbf{D}_S$  was applied to the same conditions shown in Figs. 2, 3(a) and 3(b). Table 1 shows the standard deviation of deformation components obtained by the DICM comparing those with and without eliminating the effect of time-independent distortions. The comparison reveals that correcting the time-independent distortion,  $\mathbf{D}_S$ , improves the accuracy of the measured displacement. However, the effect of time-dependent distortion,  $\mathbf{D}_T$ , remains.

Table 1: Standard deviation of deformation components in the measured region. The subset size  $M$  is 10 pixels and the magnification is  $2.5 \mu\text{m}/\text{pixel}$ .

	$u$ (pixel)	$\partial u/\partial x$ (-)	$\partial u/\partial y$ (-)	$v$ (pixel)	$\partial v/\partial x$ (-)	$\partial v/\partial y$ (-)
Stationary state, $\mathbf{t}_{\text{pre}} = (0 \mu\text{m}, 0 \mu\text{m})^T$ .						
None + $\mathbf{D}_S$ correct.	0.033	0.0021	0.0048	0.012	0.0016	0.0018
+ $\mathbf{D}_S$ + $\mathbf{D}_T$ correct.	0.033	0.0021	0.0048	0.012	0.0016	0.0018
	0.018	0.0019	0.0025	0.012	0.0016	0.0017
Translation, $\mathbf{t}_{\text{pre}} = (50 \mu\text{m}, 0 \mu\text{m})^T$ .						
None + $\mathbf{D}_S$ correct.	0.088	0.0042	0.0069	0.0024	0.0035	0.0036
+ $\mathbf{D}_S$ + $\mathbf{D}_T$ correct.	0.045	0.0042	0.0069	0.0023	0.0036	0.0037
	0.038	0.0042	0.0055	0.0023	0.0036	0.0037
Translation, $\mathbf{t}_{\text{pre}} = (50 \mu\text{m}, 50 \mu\text{m})^T$ .						
None + $\mathbf{D}_S$ correct.	0.051	0.0034	0.0062	0.044	0.0032	0.0065
+ $\mathbf{D}_S$ + $\mathbf{D}_T$ correct.	0.044	0.0034	0.0061	0.024	0.0031	0.0038
	0.031	0.0033	0.0040	0.024	0.0031	0.0038

Both the detection and the removal of time-dependent distortion,  $\mathbf{D}_T$ , by the proposed method were verified for a pair of images without any motions or deformations. The main part of the measured displacement was considered to be the difference in the time-dependent distortions between applied images, as shown in Fig. 2. To quantify the time-dependent distortion in each image, we prepared separately the images scanned in two orthogonal directions for the reference image and the deformed image. Because the scanning direction of the LSM system is fixed to the horizontal direction, the specimen was rotated approximately 90 degrees on a

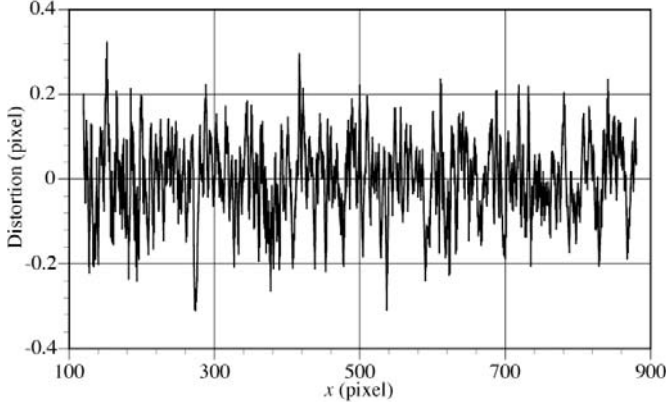


Figure 7: Distortion function of  $D_{Tx}$  estimated for the condition shown in Fig. 2 (in a stationary statement). The subset size  $M$  is 75 pixels, and the magnification is  $2.5 \mu\text{m}/\text{pixel}$ .

turntable to change the scan direction. The obtained function  $\mathbf{D}_T$  is shown in Fig. 7. In this case, the rotation angle defined by Eq. (19) was  $90.7 \pm 0.2$  degrees:

$$\theta = \sin^{-1} \left[ \frac{1}{2} \left( \frac{\partial v}{\partial x} - \frac{\partial u}{\partial y} \right) \right] \quad (19)$$

The estimated value of  $\mathbf{D}_T$  is not sensitive to the accuracy of the rotation angle. We detected  $\mathbf{D}_T$  with rotations of 89.8 degrees and 79.2 degrees, obtaining slightly different values. Displacements of the stationary statements measured using both obtained  $\mathbf{D}_T$  values showed similar standard deviations (the ratio  $\sigma_{79.2}/\sigma_{89.8} = 1.02$ ), which are the same with the errors of measurements. Thus, the proposed procedure is not sensitive to the accuracy of the rotation angle.

Image correction using both the distortion map  $\mathbf{D}_S$  and the different values for the distortion function  $\mathbf{D}_T$  was used to calibrate the displacement measured in Figs. 2, 3(a) and 3(b). The standard deviation of the deformation components obtained by the DICM in conjunction with the correction of both distortions,  $\mathbf{D}_S$  and  $\mathbf{D}_T$ , is shown in Table 1. The distributions of the errors of relative displacement measured by the DICM with the correction of  $\mathbf{D}_S$  and  $\mathbf{D}_T$  are shown in Fig. 3(c). These results indicate that the DICM in conjunction with the proposed image correction technique is capable of eliminating both distortions,  $\mathbf{D}_S$  and  $\mathbf{D}_T$ , in an LSM image and can also measure full-field displacement within 0.04 pixels of the standard deviation.

#### 4.2 Thermal strain in a copper specimen

To examine the applicability of strain measurement under thermal loading, the thermal strain in a copper specimen ( $24 \times 6 \times 0.25$  mm) was measured by the proposed method during heating from  $27.7^\circ\text{C}$  to  $70.5^\circ\text{C}$ . The coefficient of thermal expansion of copper is 17.1 ppm/K. The relative error between the measured strain and the reference strain is shown in Fig. 8. The proposed correction method decreased the error of the  $\varepsilon_{xx}$  strain field, which is related to distortion  $\mathbf{D}_S$ , and eliminated the striped error pattern in the  $\varepsilon_{xy}$  strain field, which was caused by distortion  $\mathbf{D}_T$ . Only the random error remained in the corrected distribution of strain. The standard deviation of relative error between the reference strain and the measured strain is less than 0.0003. These results prove the sufficient applicability of the proposed system to the measurement of the distribution strain caused by temperature change.

#### 4.3 Thermal strain of a print circuit board

The strain field in the cross-section of a print circuit board (PCB) during a thermal cycle test was measured using the present system in order to validate its applicability for a microstructure. The configuration of the PCB is shown in Fig. 9. During a thermal cycle test, the PCB warped due to the mismatch of coefficients of thermal expansion of the components. Fig. 10 shows the variation of the curvature due to the macroscopic warpage during the thermal cycle test, which was measured using a laser focus displacement meter. Fig. 11(a) shows the interest region of the PCB at the magnification of  $1.3 \mu\text{m}/\text{pixel}$ , and Figs. 11(a)(b)(c) shows the strain field measured by the DICM system during the heating process from  $25.6^\circ\text{C}$  to  $85.9^\circ\text{C}$ . The orientation of the fiber influenced the distribution of the strain. Normal strain  $\varepsilon_y$  on the section of glass fiber is obviously smaller than the normal strain applied to other areas. However, the distribution of  $\varepsilon_x$  and  $\varepsilon_{xy}$  are too complicated to be interpreted as a simple mechanism.

The distribution of strain was measured in the region coinciding with one period of the fiber arrangement along the  $x$ -axis. The mean value of the strain  $\varepsilon_x$  through one period of fiber arrangement along the  $x$ -axis was calculated. Because of its linearity, the macroscopic curvature of the PCB can be expected using the classic beam theory. The PCB curvature with temperature expected from the homogenized strain corresponded well with that measured using a laser focus displacement meter, as shown in Fig. 10. This result indirectly proved the accuracy of the measured distribution of strain at the cross-section of a PCB.

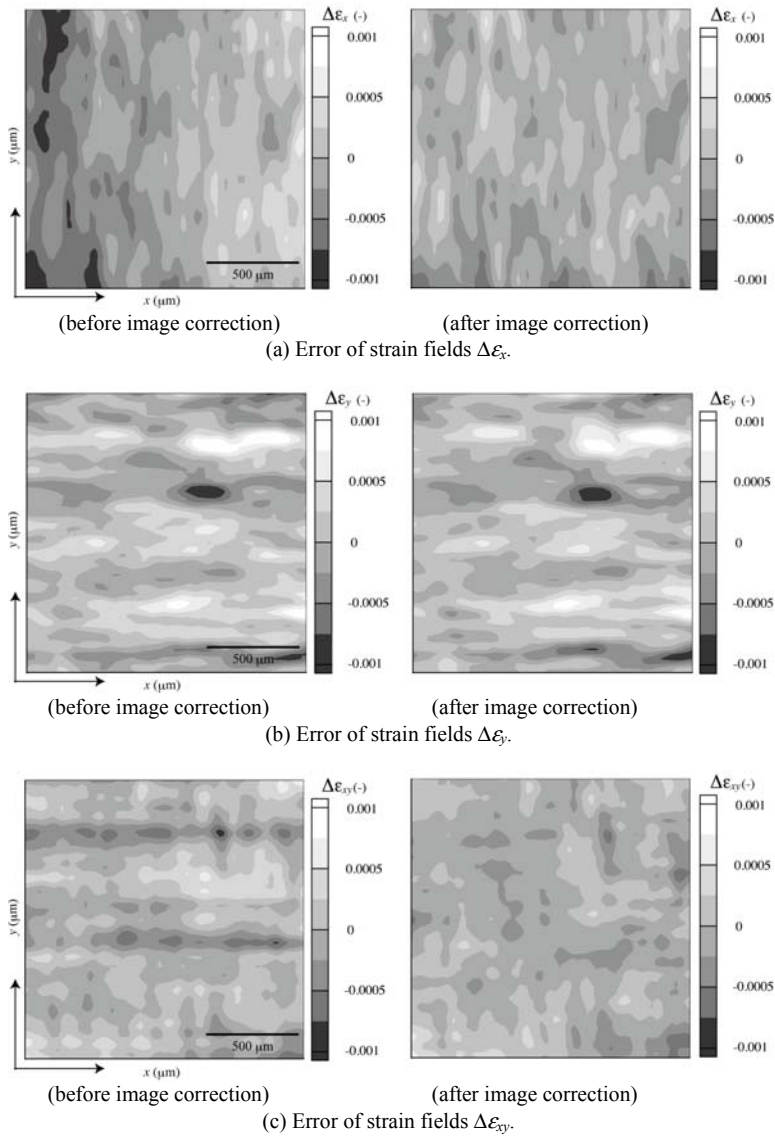


Figure 8: The relative error of thermal strain in a copper specimen during heating. The reference strain corresponds to a thermal expansion of  $\alpha\Delta T$  for  $\alpha g$  17.1 ppm/K and  $\Delta T = 42.8$  K. The subset size  $M$  is 50 pixels.

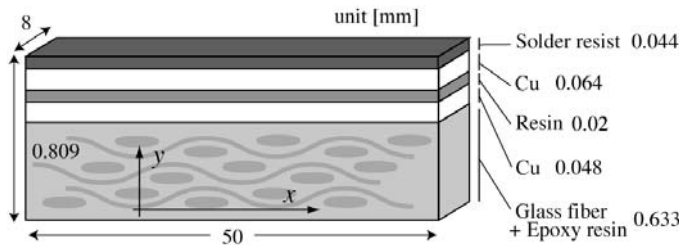


Figure 9: Configuration of a printed circuit board (PCB).

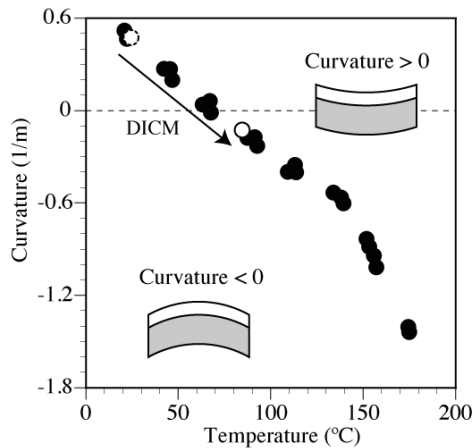


Figure 10: Curvature of a PCB measured by a displacement meter after pre-heating. There is no history dependence after heating to the glass transition point (around 150°C).

## 5 Conclusions

We developed an LSM image correction method that removes the time-dependent and time-independent distortions,  $\mathbf{D}_S$  and  $\mathbf{D}_T$ , in an image obtained by an LSM for the DICM. The conclusions of the present study are as follows:

- 1) Experimental results using a pair of images with and without motion verified the validity of the assumption that there are both time-dependent and time-independent distortions,  $\mathbf{D}_S$  and  $\mathbf{D}_T$ , in an LSM image.
- 2) The proposed correction method effectively improves the accuracy of the displacement measured using the DICM for imaging systems such as LSMs which allow complicated distributing distortions. After overall corrections for both

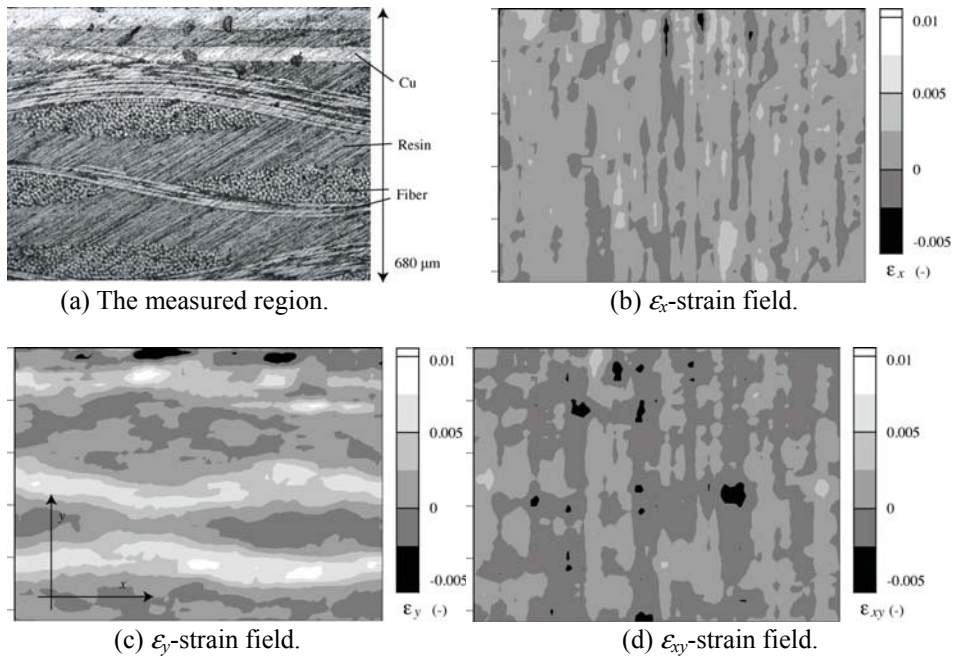


Figure 11: Results of strain measurement after a change in temperature from 25.6°C to 85.9°C.

distortions, the standard deviation of the measured displacements was 0.04 pixel.

- 3) The distribution of thermal strain in a copper specimen measured by the present method was sufficiently consistent with reference values, proving the applicability of the developed system for thermal deformation.
- 4) The thermal strain of a PCB during a thermal cycle test was measured using the present method, and although the distribution was complicated, the results were accurately related to the macroscopic warpage of the PCB.

**Acknowledgement:** We gratefully acknowledge the support of (a) Murata Manufacturing Co., Ltd., (b) a grant of the Fukuoka Project in the Cooperative Link of Unique Science and Technology for Economy Revitalization (CLUSTER) of the Ministry of Education, Culture, Sports, Science and Technology (MEXT), and (c) a Grant-in-Aid for Scientific Research from the Japan Society for the Promotion of Science. The technical assistance provided by Takashi Fujii and Akira Saito is also deeply appreciated.

**References**

- Ali, H.** (1997): Stress-Induced Parametric Shift in Plastic Packaged Devices, *IEEE Transactions on Components, Packaging, and Manufacturing Technology-Part B*, vol. 20, no. 4, pp. 458-462.
- Brown, D. C.** (1971): Close-Range Camera Calibration, *Photogrammetric Engineering*, vol. 37, no. 8, pp. 855-866.
- Bruck, H. A.; McNeill, S. R.; Sutton, M. A.; Peters III, W. H.** (1989): Digital Image Correlation Using Newton-Raphson Method of Partial Differential Correlation, *Experimental Mechanics*, vol. 29, pp. 261-267.
- Guo, Y.; Lim, C. K.; Chen, W. T.; Woychik, C. G.** (1993): Solder Ball Connect (SBC) Assemblies under Thermal Loading: I. Deformation Measurement via Moiré Interferometry, and Its Interpretation, *IBM J. Res. Develop.*, vol. 37, no. 5, pp. 635-647.
- Hamada, A.; Furusawa, T.; Saito, N.; Takeda, E.** (1991): A New Aspect of Mechanical Stress Effects in Scaled MOS Devices. *IEEE Transactions on Electron Devices*, vol. 38, no. 4, pp. 895-900.
- Ikeda, T.; Arase, I.; Ueno, Y.; Miyazaki, N.** (2000): Strength Evaluation of Electronic Plastic Packages Using Stress Intensity Factors of V-Notch, *CMES: Computer Modeling in Engineering & Sciences*, vol. 1, no. 1, pp. 91-97.
- Lancaster, P.; Salkauskas, K.** (1981): Surfaces Generated by Moving Least Squares Methods, *Mathematics of Computation*, vol. 37, no. 155, pp. 141-158.
- Laraba-Abbes, F.; Ienny, P.; Piques, R.** (2003): A New 'Tailor-made' Methodology for the Mechanical Behaviour Analysis of Rubber-like Materials: I. Kinematics Measurements Using a Digital Speckle Extensometry, *Polymer*, vol. 44, pp. 807-820.
- Li, X.; Xu, W.; Sutton, M. A.; Mello, M.** (2006): Nanoscale Deformation and Cracking Studies of Advanced Metal Evaporated Magnetic Tapes Using Atomic Force Microscopy and Digital Image Correlation Techniques, *Materials Science and Technology*, vol. 22, no. 7, pp. 835-843.
- Lucchese, L.** (2005): Geometric Calibration of Digital Cameras through Multi-view Rectification, *Image and Vision Computing*, vol. 23, pp. 517-539.
- Nie, Y. F.; Atluri, S. N.; Zuo, C. W.** (2006): The Optimal Radius of the Support of Radial Weights Used in Moving Least Squares Approximation, *CMES: Computer Modeling in Engineering & Sciences*, vol. 12, no. 2, pp. 137-147.
- Schreier, H. W.; Sutton, M. A.** (2002): Systematic Errors in Digital Image Correlation Due to Undermatched Subset Shape Functions, *Experimental Mechanics*, vol. 40, no. 3, pp. 303-310.

**Schreier, H. W.; Garcia, D.; Sutton, M. A.** (2004): Advances in Light Microscope Stereo Vision, *Experimental Mechanics*, vol. 44, no. 3, pp. 278-289.

**Sun, Y.; Pang, J. H L** (2006): AFM Image Reconstruction for Deformation Measurements by Digital Image Correlation, *Nanotechnology*, vol. 17, pp. 933-939.

**Sutton, M. A.; Li, N.; Garcia, D.; Cornille, N.; Orteu, J. J.; McNeill, S. R.; Schreier, H. W.; Li, X.** (2006): Metrology in a Scanning Electron Microscope: Theoretical Developments and Experimental Validation, *Measurement Science and Technology*, vol. 17, pp. 2613-2622.

**Sutton, M. A.; Li, N.; Joy, D. C.; Reynolds, A. P.; Li, X.** (2007): Scanning Electron Microscopy for Quantitative Small and Large Deformation Measurements Part I, *Experimental Mechanics*, vol. 47, pp. 775-787.

**Takashima, S.; Nakagaki, M.; Miyazaki, N.** (2007): An Elastic-Plastic Constitutive Equation Taking Account of Particle Size and Its Application to A Homogenized Finite Element Analysis of A Composite Material, *CMES: Computer Modeling in Engineering & Sciences*, vol. 20, no. 3, pp. 193-202.

**Tay, A. A. O.; Goh, K. Y.** (2003): A Study of Delamination Growth in the Die-Attach Layer of Plastic IC Packages under Hygrothermal Loading During Solder Reflow, *IEEE Transactions on Device and Materials Reliability*, vol. 3, no. 4, pp. 144-151.

**Yan, J. H.; Sutton, M. A.; Deng, X.; Cheng, C. S.** (2007): Mixed-mode Fracture of Ductile Thin-sheet Materials under Combined In-plane and Out-of-plane Loading, *Int. J. Fract.*, vol. 144, no. 4, pp. 297-321.

**Yoneyama, S.; Kitagawa, A.; Kitamura, K.; Kikuta, H.** (2006): In-Plane Displacement Measurement Using Digital Image Correlation with Lens Distortion Correction, *JSME International Journal, Series A*, vol. 49, no. 3, pp. 458-467.

